Journal of Colloid and Interface Science 660 (2024) 522–533

Contents lists available at ScienceDirect

Journal of Colloid And Interface Science

journal homepage: www.elsevier.com/locate/jcis

Regular Article

A new consistent modeling framework for the competitive adsorption of humic nanoparticles and oxyanions to metal (hydr)oxides: Multiple modes of heterogeneity, fractionation, and conformational change

Yun Xu [a,b,1], Yilina Bai [a,1], Tjisse Hiemstra [a], Liping Weng [a,c,*]

[a] Soil Chemistry and Chemical Soil Quality, Wageningen University & Research, 6708 PB Wageningen, The Netherlands
[b] State Environmental Protection Key Laboratory of Soil Health and Green Remediation, College of Resources and Environment, Huazhong Agricultural University, 430070 Wuhan, China
[c] Agro-Environmental Protection Institute, Ministry of Agriculture, 300191 Tianjin, China

GRAPHICAL ABSTRACT

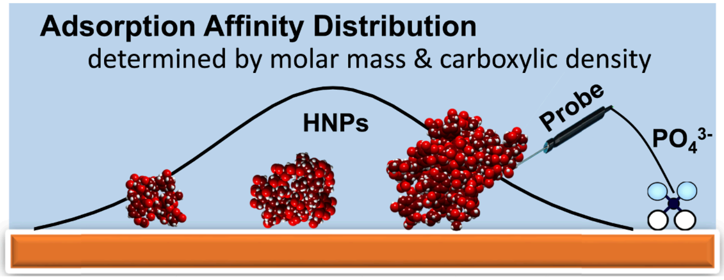

ARTICLE INFO

Keywords:
Nanoparticles
Heterogeneity
Size exclusion chromatography
Fractionation
LCD model
Affinity distribution
Spatial distribution
Electrostatic potential
Conformational change

ABSTRACT

Hypothesis: The competitive interaction of oxyanions and humic nanoparticles (HNPs) with metal (hydr)oxide surfaces can be used to trace the ligand and charge distribution of adsorbed HNPs in relation to heterogeneity, fractionation, and conformational change.
Experiments: Batch adsorption experiments of HNPs on goethite were performed in the absence and presence of phosphate. The size of HNPs was measured with size exclusion chromatography. The Ligand and Charge Distribution (LCD) model framework was further developed to describe the simultaneous interaction of HNPs and phosphate with goethite.
Findings: Preferential adsorption decreases the mean molar mass of adsorbed HNPs, independent of the phosphate presence, showing a linear dependency on the adsorbed HNPs fraction. Phosphate ion can be used as a probe to trace the distribution of functional groups and the variation in affinity of HNPs. The spatial distribution of adsorbed HNPs is driven by the potential gradients in the electrical double layer, which changes the conformation of the adsorbed HNPs. At the particle level, the adsorption of heterogeneous HNPs has an affinity distribution, which can be explained by the variation in molar mass (kDa) and density of the functional groups (mol

---

[*] Corresponding author at: Soil Chemistry and Chemical Soil Quality, Wageningen University & Research, 6708 PB Wageningen, The Netherlands.
E-mail address: liping.weng@wur.nl (L. Weng).
[1] These authors contribute equally.

https://doi.org/10.1016/j.jcis.2024.01.078
Received 13 July 2023; Received in revised form 9 January 2024; Accepted 11 January 2024

kg^{-1}) of the HNPs. The presented model can simultaneously describe the competitive adsorption of HNPs and phosphate in a consistent manner.

1. Introduction

Natural organic matter (NOM) and metal (hydr)oxides are highly reactive materials [1], which can strongly interact with each other and can bind inorganic as well as organic constituents in both natural environments [2–4] and industrial processes [5–7]. NOM consists of a broad spectrum of organic molecules having dimensions ranging from approximately 1 to 10 nm and are therefore referred to as humic nanoparticles (HNPs) [8]. Humic nanoparticles (HNPs) are intrinsically heterogeneous, varying in composition, structure, and charge [9]. HNPs consist of components of different polarities. The highly polar parts have reactive functional groups that can develop pH-dependent charge under typical solution conditions [9–11]. Due to the compositional complexity and inherent heterogeneity of HNPs, understanding and describing their adsorption behaviors to metal (hydr)oxides is a great challenge especially because specific fractions of HNP are preferentially bound to metal (hydr)oxide surfaces, known as molecular fractionation. In addition, HNPs have a flexible structure, allowing conformational changes upon adsorption in charged interfaces of metal (hydr)oxides. If inorganic ions are additionally bound in these interfaces, modeling the adsorption of HNPs and their interactions with inorganic ions is even more challenging.

For describing the adsorption of HNPs to metal (hydr)oxides, surface complexation models have been developed [12–15]. The Ligand and Charge Distribution (LCD) model is a framework in which various aspects of the interaction are treated using several concepts [13]. The word "ligand" is used for the functional groups of HNPs that interact with protons and metal ions. Chemical heterogeneity of the ligands of HNPs is described in the LCD model with the concept of the Non-Ideal Competitive Adsorption (NICA) model [16]. In this approach, the affinity of the ligands (i.e., functional groups) for ion interaction, including surface sites on oxides, is described by assuming a continuous distribution of affinities. Moreover, at the particle level, HNPs may exhibit heterogeneity because of their polydisperse nature, showing a distribution in molar mass and size. The recently extended LCD model (LCD_{ex}) [17] considers molecular fractionation of HNPs by adsorption that changes the mean molar mass of adsorbed HNPs [18–21]. However, the polydispersity of adsorbed HNPs has not been included in the LCD concept, as the molar mass is assumed to be fixed to an average value. Along with changes in the molar mass of HNPs, variations in hydrophobicity [22,23], aromaticity [24,25], and aliphatic groups [7,21] as well as carboxylic group density as a function of molar mass [19] may also play a role in changing the overall adsorption affinity to metal (hydr)oxides. This can affect surface properties and the adsorption of other ions on oxides.

Metal (hydr)oxides not only interact with HNPs, but also with oxyanions such as phosphate, arsenate, and others [26–28]. In multicomponent systems, this may result in strong competition between HNPs and oxyanions for binding to metal (hydr)oxides [29–33]. Due to competition, it is expected that ligands of HNPs with a high affinity will be preferred over those with a low affinity in the formation of surface complexes. This variation in the affinity of ligands can be described with the NICA model that is implemented in the LCD framework [13]. However, in HNPs, the ligands are not equally distributed over various particles in terms of types, affinities, and density [34]. It implies that heterogeneity exists not only at the level of the ligands but also at the level of the particle. This aspect has been ignored in the LCD models developed so far (i.e., the initial LCD model (LCD_{ini}) [13] and its extended version (LCD_{ex}) [17], while oxyanions such as phosphate can potentially serve as a probe to create a strong competitive situation, which can better reveal the variations in affinity of HNPs.

In addition to multiple modes of heterogeneity, HNPs are not rigid entities and may alter their molecular conformation upon adsorption. At low loading and low pH, HNPs tend to preferentially occupy the compact part of the electric double layer (EDL), while at a higher loading, HNPs may also occupy part of the diffuse layer outside the compact part of the interface [33]. The recently extended LCD model (LCD_{ex}) [17] considers HNPs as a flexible soft matter that may change its molecular conformation depending on the gradient of electrostatic potentials in the EDL. This version of the LCD model (LCD_{ex}) can successfully describe the adsorption of HNPs to goethite as a function of pH, ionic strength, and loading [17]. However, the applicability of this approach for systems that also contain oxyanions has not been validated.

In the present study, the adsorption of HNPs to goethite in the absence and presence of phosphate will be compared experimentally. In this approach, phosphate ion (PO_4^{3-}) is used as a probe to trace the distribution of the charged functional groups of HNPs in the interface due to its sensitivity to the changes in the EDL profile. Moreover, by adding phosphate, one can deliberately change the EDL profile, which affect the adsorption of HNPs. Additionally, it provides information about the affinity distribution of HNPs, as mentioned above. By probing with PO_4^{3-}, we hope to elucidate the spatial distribution of the ligands in the interface and its change with conditions, thereby improving our insights into the molecular conformation of adsorbed HNPs. We also like to unravel the various modes of heterogeneity and the affinity that influence the adsorption and interfacial distribution of HNPs. The challenge is to develop a consistent model framework for competitive adsorption that can be used to understand and predict the interaction of oxyanions and HNPs with metal (hydr)oxides.

2. Materials and methods

2.1. Materials

In this study, HNPs will be represented by humic acid (HA), extracted from a soil sample collected from the Bh-horizon of a podzol soil in Tongbersven forest, close to Oisterwijk, Tilburg, the Netherlands (51°34′46″N 5°14′48″E). It was purified according to the protocols of the International Humic Substances Society (IHSS). The carbon content of HA (58 %) was determined by measuring total organic carbon (TOC) in a solution with a known mass of HA (Sievers 900, GE, USA). The average molar mass (M_w, 17 kDa) was measured with size exclusion chromatography (SEC) in combination with UV–Vis spectrometry (see below).

Goethite, a crystalline metal (hydr)oxide important in the natural environment, was prepared according to Hiemstra et al. [35]. In this approach, goethite was prepared by slowly neutralizing freshly prepared 0.5 M $Fe(NO_3)_3\cdot 9H_2O$ with 2.5 M NaOH at approximately 10 % neutralization per hour to a pH of 12. The suspension was aged for 4 days at 60 °C and subsequently dialyzed with ultrapure water for 2 weeks. The BET-N_2 specific surface area (SSA) of this goethite is 99 $m^2\ g^{-1}$ and the pristine point of zero charge (PZC) is pH = 9.3 [36].

2.2. Adsorption experiment

Three batch adsorption experiments (Exp) were carried out in the presence of 3.0 g L^{-1} goethite in an electrolyte background of 0.01 M NaCl. In Exp A (pH 4), the phosphate addition (x = 0–0.45 mM phosphate as $NaH_2PO_4\cdot 2H_2O$, expressed as $x$$PO_4$) was varied at a constant HA addition (y = 200, 350, or 450 mg L^{-1}, noted as $x$$PO_4$ + [yHA]). In Exp B (pH 4), the HA addition (x = 0–500 mg L^{-1} HA) was varied at a constant phosphate concentration (y = 0.45 mM, indexed as xHA + [$y$$PO_4$]). In Exp C, we used the same initial HA and phosphate loading as in Exp B, but the adsorption was done for pH 6. All the experiments were performed in gas-tight polyethylene centrifugation vessels with N_2 gas flushing during the preparation of the suspensions to minimize the influence of CO_2. The additions were in the order of NaCl, HA, phosphate, and goethite. Acid (0.1 M HCl) or base (0.1 M NaOH) was added to adjust the pH of the suspension to 4 or 6. Finally, ultra-pure water was added to top up the total volume to 30 mL. The prepared suspensions were shaken in a temperature-controlled room (20 °C) for 7 days to reach a pseudo-equilibrium. The pH was readjusted after the first 48 h if needed. After shaking, all suspensions were centrifuged at 18,000 g for 30 min. The supernatant was filtered over a 0.45 μm membrane filter and the final pH in the supernatant was measured, which was 4.0 ± 0.1 or 6.0 ± 0.1. The filtrate was used for TOC analysis (SFA-TOC analyzer, SKALAR, Netherlands), size exclusion chromatography (SEC) analysis (details in Section 2.3), and analysis of the phosphate concentration with an SFA-PO_4 analyzer (SKALAR, Netherlands).

2.3. SEC analysis

The size exclusion chromatograms of HA before and after adsorption in one series in Exp A ($x$$PO_4$ + [450 mg/LHA]) and Exp B (xHA + [0.45 mM PO_4]) (both at pH 4) were measured on an HPLC system with an SEC column (BioSep-SEC-S2000 column) linked to a diode array UV detector (PN3241 UV detector, Postnova Analytics, Germany). A volume of 100 μL of the sample solution was injected. The samples were carried by a pH buffer solution with a 1:1 mixture of 0.1 M NaH_2PO_4 and Na_2HPO_4 (pH = 6.9) at a flow rate of 1.0 mL min^{-1}. Polystyrene sulfonates (PSS) with a molar mass of 1.3, 13, 80, 200, and 280 kDa, purchased from Sigma Aldrich, Switzerland, were used as SEC standards (Fig. S1) to derive the molar masses of the HA samples. The reported molar mass values are consistent with the mass density of the PSS used (~800 kg m^{-3}). The mean mass-based (M_w) and number-based (M_n) molar masses were calculated with respectively Eq.1a and 1b.

$$M_w = \frac{\sum_{i=1}^{N} f_i M_i^2}{\sum_{i=1}^{N} f_i M_i} = \frac{\sum_{i=1}^{N} h_i M_i}{\sum_{i=1}^{N} h_i} \tag{1a}$$

$$M_n = \frac{\sum_{i=1}^{N} f_i M_i}{\sum_{i=1}^{N} \frac{f_i M_i}{M_i}} = \frac{\sum_{i=1}^{N} h_i}{\sum_{i=1}^{N} \frac{h_i}{M_i}} \tag{1b}$$

where f_i is the frequency of the number of molecules, M_i is the molar mass of particles at elution volume I or at retention time i, calculated from the calibration curve., N is the number of molecular fractions according to the molar mass, and h_i is the absolute absorbance at 254 nm.

The SEC chromatograms of HA in the adsorption phase were calculated from the difference in the chromatograms of HA in solution before and after adsorption. The polydispersity index ($\rho \geq 1$) was calculated as M_w/M_n. For a pure substance with a single size, $\rho \equiv 1$, whereas $\rho > 1$ for a mixture of molecules [37]. The SEC results of Exp A ($x$$PO_4$ + [450 mg/L HA]) are summarized in Table S1.

3. Model theory

Our model is based on four basic concepts used in different calculation modules, namely Non-Ideal Competitive Adsorption coupled with Donnan (NICA-Donnan), Non-Ideal Competitive Adsorption coupled with Ligand Distribution (NICA-LD), Charge Distribution MUlti-Site Ion Complexation (CD-MUSIC), and Adsorption and Adaption (ADAPT) [13]. The model calculations were implemented in the ORCHESTRA software package [38]. During the calculation, the values of the unknown variables are estimated by a Newton-Raphson iteration procedure. This iterative process is finished when the calculated solution of all equations for unknown variables falls within the specified tolerances. The various modeling concepts will be detailed below.

3.1. Non-ideal competitive adsorption behaviors of HNPs

In the LCD model framework, the NICA module describes the specific binding of ions or sites to the two types of reactive ligands (carboxylic and phenolic types) of HNPs, accounting for the intrinsic chemical heterogeneity of the ligands and ion-specific non-ideality [16]. In the solution phase, the non-specific coulombic binding of electrolyte ions by HNPs is calculated using the Donnan model approach. Collected acid-base titration data [36] have been used to derive the NICA-Donnan parameters, comprising the overall site densities of the carboxylic ($Q_{max,1}$) and phenolic ($Q_{max,2}$) groups, the median protonation constants ($\log\widetilde{K}_{H,1}$, $\log\widetilde{K}_{H,2}$) and the intrinsic heterogeneity parameters (m_1, m_2) of the carboxylic and phenolic groups [39]. These can be found in Table S2. The NICA-Donnan module requires the input of the volume fraction of HNPs in solution ($\phi_{p,sol}$), which is iteratively calculated with the ADAPT module. The NICA-Donnan module yields the average chemical state of the HNPs in the solution (i.e., protonated, deprotonated), and calculates the Boltzmann factor for the Donnan phase, which will be used iteratively in the ADAPT module calculations.

3.2. Interfacial distribution of ligands

The ligand distribution (LD) of HNPs is combined with the NICA model (NICA-LD module) to calculate the interaction of the reactive ligands (carboxylic and phenolic groups) of HNPs in the adsorption phase with ions and surface sites of oxides. It is assumed that the NICA model parameters for the adsorbed HNPs remain the same as for the HNPs in the solution. For the formation of the innersphere complexes ($\equiv FeOOCR^{-0.5}$) of the carboxylic type of ligands ($RCOO^-$) of adsorbed HNPs with the metal ion of the singly coordinated surface groups ($\equiv FeOH_2^{+1/2}$) of goethite, we used an optimized complexation constant of $\log\widetilde{K}_{s,1} = -1$ [40]. The negative charge of the carboxylic ligand ($\equiv RCOO^-$) in the reaction (Eq. (2)) is evenly distributed between the 0- and 1-plane.

$$\equiv FeOH_2^{+0.5} + \equiv RCOO^- \Leftrightarrow \equiv FeOOCR^{-0.5} + H_2O;\ \log\widetilde{K}_{S,1} = -1 \tag{2}$$

For large HNPs such as HA, only a part of the reactive ligands can be accommodated in the Stern layers of the EDL, while the remaining part can protrude, entering the diffuse layer [33] (Fig. 1). Based on the position of HNPs in the interface, three fractions of their reactive ligands are distinguished (f_{0+1}, f_2, and f_d). The corresponding charge is located at respectively the surface and the first Stern plane (0- & 1-plane), the second Stern plane (2-plane), and an adsorption plane located at a chosen distance of Δx from the head of the diffuse layer (DL). The charge of ligands of HNPs outside the compact part of the double layer is attributed to the d-plane. The charge of electrolyte ions in the Δx space between the 2-plane and d-plane is also attributed to the d-plane. Beyond the d-plane, the counter- and co-ions are treated according to the Gouy-Chapman theory [41,42].

In our earlier work [17], the spatial distribution was defined by the following set of equations:

$$f_{0+1} + f_2 + f_d = 1 \tag{3a}$$

$$R = f_{0+1}/(f_{0+1} + f_2) \tag{3b}$$

$$f_d = \frac{\Gamma_{tot} - \Gamma_{MST}}{\Gamma_{tot}};\ f_d = 0 \text{ when } \Gamma_{tot} < \Gamma_{MST} \tag{3c}$$

$$\theta_s = \Gamma_{MST}/\Gamma_{MST}^{o} \tag{3d}$$

where f_{0+1} is the fraction of the reactive ligands of HNPs in the first Stern layer divided over 0- and 1-plane. These ligands are protonated, deprotonated, or form innersphere complexes. The second fraction of reactive ligands (f_2) is attributed to the 2-plane. The remaining fraction

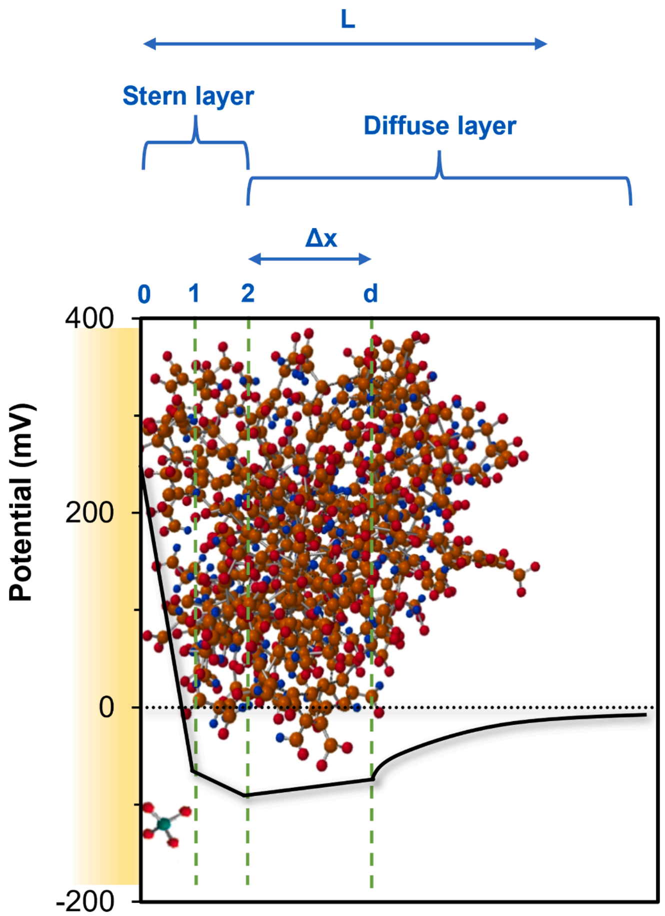

Fig. 1. Schematic representation of the interfacial adsorption of a soft HNP and phosphate onto a metal (hydr)oxide surface, showing the electrostatic potential profile in the electrical double layer (EDL) for 0.01 M NaCl background of pH 4, calculated with the Ligand and Charge Distribution framework for consistent modeling of the competitive adsorption (LCD_{cc}) for a specific loading of HA and phosphate. The x-axis reflects the distance from the interface. The charge of the HA ligands is distributed over four electrostatic planes (see text). L is the layer thickness of the adsorbed HA being $L = 2\ \Delta x + d_{ST}$ in which Δx is the distance from the 2-plane to the d-plane and d_{ST} is the thickness of the Stern layer region (~0.8 nm). The typical value of L is about 3 nm. The amount of salt ions located in the layer between the 2- and d-plane has been calculated using the average potential of both planes. the corresponding charge was attributed to the d-plane.

of reactive ligands (f_d) is present in the diffuse layer (DL), where it is attributed to an adsorption plane (d-plane) located halfway of the layer thickness of the adsorbed fraction in the DL (Fig. 1).

As a first approach (LCD_{ex} [17]), the ratio of the fractions in the Stern layers (Eq. (3b)) was fixed to $R = 0.5$ by assuming $f_{0+1} = f_2$. However, in the present study, PO_4^{3-} ions have been used to probe the ligand distribution in the compact part of the EDL, showing (Section 4.3) that R does not have a single value. Therefore, R is changed into an adjustable parameter.

According to previous modeling, HNP adsorption starts by first occupying the compact part of the Stern layer space (between 0- and 2-plane) to a maximum value (Γ_{MST}), before employing the diffuse layer space. This is defined in Eq. (3c), in which Γ_{tot} is the total amount of adsorbed HNPs. The added constraint indicates that the diffuse layer remains unoccupied ($f_d = 0$) as long as $\Gamma_{tot} < \Gamma_{MST}$.

Previous explorations with the LCD_{ex} model [17] indicated that the maximum adsorption of HNPs in the Stern layer space (Γ_{MST}) is generally less than the physical maximum of occupation ($\Gamma^{o}_{MST} \sim 1$ mg m^{-2}). The latter can be calculated by considering the adsorbed HNPs as a structureless material that can fill the Stern layer space entirely as if it is a gel. Generally, the ratio $\Gamma_{MST}/\Gamma^{o}_{MST}$ (Eq. (3d)) is less than 1, meaning that the adsorbed HNPs are structured and shaped. Modeling has shown that the relative occupation $\Gamma_{MST}/\Gamma^{o}_{MST}$ is condition-dependent [17]. The ratio of $\Gamma_{MST}/\Gamma^{o}_{MST}$ can be linked to the electrostatic potential profile of the Stern layers.

The NICA-LD model yields the average chemical state of the HNPs in the adsorbed phase (i.e., protonated, deprotonated, inner-sphere complex), and the charge carried by HNPs, which will be used iteratively in the ADAPT and CD-MUSIC module.

3.3. Distribution of charge and electrostatic potentials

The adsorption of charged entities by metal (hydr)oxides leads to a charged interface that is handled in the Charge Distribution MUlti-Site Ion Complexation (CD-MUSIC) module [43]. The basic model parameters can be found in Table S3. For the HNPs, the input in the CD-MUSIC module is the volume fraction of the adsorbed HNPs ($\phi_{p,ads}$) calculated by the ADAPT, and the average chemical state of the adsorbed HNPs calculated with the NICA–LD module, yielding the charge in each plane, carried by the ligands of the adsorbed HNPs.

Based on the charge, the potentials at 0-, 1-, and 2-planes (ψ_0, ψ_1, ψ_2) are calculated using classical Stern layer condenser formulations. The capacitances of different regions of the Stern layer can be found in Table S3. HNPs may also employ the diffuse layer, adding charge that is attributed to an additionally defined d-plane at a distance Δx from the compact part of the EDL (Fig. 1). The potential at this additional plane (ψ_d) depends on its location, following Eq. (4).

$$\left(\frac{\psi_d - \psi_2}{\Delta x}\right) = \frac{\sigma_{DL}}{\varepsilon_r \varepsilon_0} \tag{4}$$

in which σ_{DL} (C m^{-2}) is the excess charge in the diffuse layer (DL) between the 2-plane and infinity, including the charge of the electrolyte ions and HNPs in the inner DL (2- and d-plane) and the charge of the electrolyte ions in the outer DL (outside d-plane). In our model, the d-plane is located at a distance Δx, which is set at half of the maximum distance of HNPs in the DL region (Fig. 1). If L is the maximum layer thickness of adsorbed HNPs, Δx can be calculated with $\Delta x = ½\ (L – d_{ST})$ in which d_{ST} is the thickness of the Stern layer (~0.8 nm). The total layer thickness (L, nm) is estimated from the maximum loading of adsorbed HNPs (mg m^{-2}) measured at each ionic strength and the mass density of adsorbed HNPs. This density of the adsorbed fraction of HNPs has been set to 1250 kg m^{-3} [44], which is larger than the density of well-hydrated HNPs in the free solution (700 kg m^{-3} [45]) but smaller than the mass density of humic material HNPs in the dry state (1700 kg m^{-3} [46]). The in-between value chosen gives credits to some dehydration of HNPs upon adsorption, caused by innersphere complexation and the observed conformational changes, both pressuring adsorbed HNPs.

The CD-MUSIC module calculates the charge and electrostatic potentials at each electrostatic plane, which will be used in the NICA-LD module. It also calculates the adsorption of ions to metal (hydr)oxides.

3.4. Adsorption energy and heterogeneity of humic nanoparticles

Upon adsorption, HNPs adapt their ligand (or functional groups) speciation and corresponding charge to the local interfacial conditions via the adsorption and desorption of protons and other cations, as well as via ligand exchange reactions with reactive sites on the metal (hydr) oxide surfaces. The shift in their average chemical state (protonated, deprotonated, and innersphere complex) upon adsorption leads to a free energy change. The Adsorption and Adaption (ADAPT) module [13] calculates this change in free energy.

In the initial LCD (LCD_{ini}) [13] and extended LCD (LCD_{ex}) modeling [17], the well-known Langmuir expression was used to calculate the adsorption of HNPs, in which the concentration of HNPs in the adsorption (ads) and solution (sol) phase are expressed in volume fractions (ϕ), leading to:

$$\frac{\phi_{\text{ads}}}{1-\phi_{\text{ads}}} = K_{\text{o}}\phi_{\text{sol}} = K_{\text{sp}}K_{\text{nsp}}\phi_{\text{sol}} \tag{5a}$$

where K_{o} is the reaction constant, expressing the affinity. ϕ_{sol} and ϕ_{ads} are the volume fraction of HNPs in respectively the solution and adsorbed phase. The overall affinity K_{o} has a specific (K_{sp}) and non-specific (K_{nsp}) energy contribution, which can be calculated with the ADAPT module using the mean molar mass (M_{w}) and the mean density of functional groups (Q_{max}) [36] following Eqs. (5b)–(5d):

$$N_{\text{max},j,l} = Q_{\text{max},j}M_{\text{w}}f_l \tag{5b}$$

$$K_{\text{p,sp}} = \prod_{l}\prod_{j=1}^{2}\left\{\left(\frac{1-\sum\theta_{i,j,\text{sol}}}{1-\sum\theta_{i,j,\text{ads},l}}\right)^{\frac{N_{\text{max},j,l}}{n_{\text{H},j}p_j}}\right\}\left(\frac{B_{\text{D}}}{B_l}\right)^{N_{\text{max},j,l}} \tag{5c}$$

$$K_{\text{p,nsp}} = e^{-C_{i,\text{bulk}}V_{\text{D}}\frac{M_{\text{w}}}{1000}\left(B_{\text{D}}+\frac{1}{B_{\text{D}}}-2\right)} \tag{5d}$$

in which $N_{\text{max},j,l}$ (mol mol^{-1}) is the number of type j ligands ($j = 1$, carboxylic; $j = 2$, phenolic) per HNP in each layer (l); $n_{\text{H},j}$, and p_j are the NICA parameters that can be found in Table S2; $\theta_{i,j,\text{sol}}$ is the fraction of type j ligands of HNPs that are complexed with component i (protons or sites) in the solution phase; $\theta_{i,j,\text{ads},l}$ is the fraction of type j ligands of adsorbed HNPs that are complexed with component i (protons or sites) in layer (l); $C_{i,\text{bulk}}$ (mol L^{-1}) is the concentration of the electrolyte ions (monovalent) in the solution, and V_{D} (L kg^{-1}) is the volume of the Donnan phase of HNPs in solution; M_{w} is the mean molar mass (g mol^{-1}) of HNPs, which can be estimated using an empirical equation in which the molar mass is a function of the fraction of HNPs adsorbed (Table 1) [17]; B_l is the Boltzmann factor at each electrostatic plane where the charge of HNPs is located; B_{D} is the Boltzmann factor for the Donnan phase of HNPs in solution.

The above formulations are for average HNPs. However, our SEC measurements demonstrate that the molar mass of HNPs has a significant distribution around the average value. In addition, the HNPs may differ in terms of the quantity (density) and/or the quality (type) of the functional groups. In other words, one may expect heterogeneity at the particle level, leading to a distribution of affinity constants.

Using a semi-Gaussian distribution of affinities [47] with a median value $\widetilde{K}_{\text{o}}$ and a width expressed in a parameter q ($0 \leq q \leq 1$), the above Langmuir expression can be rewritten to the well-known Langmuir-Freundlich (LF) equation:

$$\frac{\phi_{\text{ads}}}{1-\phi_{\text{ads}}} = \left(\widetilde{K}_{\text{o}}\phi_{\text{sol}}\right)^q = \left(\widetilde{K}_{\text{sp}}\widetilde{K}_{\text{nsp}}\phi_{\text{sol}}\right)^q \tag{6}$$

The logarithm of the median affinity constant ($\log \widetilde{K}_{\text{o}}$) is related to the corresponding Gibbs free energy change of HNPs upon adsorption. In the present approach of consistent modeling of the adsorption of HNPs, we will apply the above LF equation (Eq. (6)). The heterogeneity of the HNPs at the particle level, expressed in the value of q, will be evaluated. For the sake of simplicity, the particle-level heterogeneity of HNPs in solution was neglected in the free energy calculation. This approach differs from previous attempts [13,17,36] in which the Langmuir approach was used (Eq. (5a)), in which heterogeneity at the particle level was ignored in modeling the adsorption of HNPs (i.e., $q \equiv 1$).

To calculate the change of free energy, or the adsorption affinity, the input is the values of the average chemical state of the HNPs in the solution phase and in the adsorption phase, as well as the Boltzmann factor in the Donnan phase and at the oxide surface. These values are the output of modules of NICA-Donnan, NICA-LD, and CD-MUSIC. With the iterations, the distribution of the HNPs in terms of the volume fraction of the particles in the solution (ϕ_{sol}) and in the adsorption phase (ϕ_{ads}) are the output of the ADAPT module.

For a good understanding of the differences between previous attempts to model the adsorption of HNPs (LCD$_{\text{ini}}$ and LCD$_{\text{ex}}$) and the new approach for consistent modeling of competitive adsorption (LCD$_{\text{cc}}$), an overview is given of the key factors of both versions of the model (Table 1).

4. Results and discussion

4.1. *Fractionation of humic nanoparticles affected by phosphate*

In the model, the energy change of an HNP with variable charge placed in an electrostatic field depends on the number of functional groups of that particle. Therefore, it is related to the molar mass of the adsorbed HNPs at a given site density [36], making it a key factor in modeling the adsorption of HNPs.

In our first experiment (Exp A), the phosphate loading was varied with fixed levels (200, 350, and 450 mg L^{-1}) of HA added. The adsorption was measured for all treatments, and SEC measurements were carried out for the treatments with 450 mg L^{-1} HA. Fig. 2a shows the corresponding chromatograms of adsorbed HA that were derived from

Table 1
Development of LCD framework over the last 20 years. Comparison of the key factors (i.e., mean molar mass, spatial distribution, particle-level heterogeneity) for the initial LCD model (LCD$_{\text{ini}}$) [13], extended LCD model (LCD$_{\text{ex}}$) [17], and consistent competitive LCD model (LCD$_{\text{cc}}$) in modeling HNPs adsorption to goethite.

Models	**Key factors in modeling***		
	Mean molar mass due to fractionation 1)	**Conformational change** 2)	**Particle-level heterogeneity (q)** 3)
LCD$_{\text{ini}}$	No fractionation	Rigid spheres	Homogeneous ($q \equiv 1$)
LCD$_{\text{ex}}$	$M_{\text{w}} = M_{\text{o}} + k$ (1- ρ_{ssr} C_{HNP}/ HNP$_{\text{tot}}$)	$\theta_{\text{S}} \sim(\psi_0 - \psi_2)$ $R \equiv 0.5$ ($f_{0+1} \equiv f_2$)	Homogeneous ($q \equiv 1$)
LCD$_{\text{cc}}$		$\theta_{\text{S}} \sim(\psi_0 - \psi_2)$ $R \sim(\psi_0 - \psi_1)$	Heterogenous ($0 < q < 1$)

1. In the LCD$_{\text{ini}}$, size fractionation of HNPs is ignored. Only a single molar mass is considered which is set equal to the measured mean molar mass of HNPs without fractionation (17 kDa in our case). Both LCD$_{\text{ex}}$ and LCD$_{\text{cc}}$ include size fractionation by adsorption, and the mean molar mass of adsorbed HNPs is found to be dependent on adsorbed HNPs fraction. M_{o} (kDa) is the molar mass of the most preferred HNPs in the adsorption, k is the fractionation factor (kDa), ρ_{ssr} is the solution-to-solid ratio (i.e., 1.0 L g^{-1} goethite), C_{HNP} (mg L^{-1}) is the concentration of HNPs in solution, and HNP$_{\text{tot}}$ (mg g^{-1}) is the total added HNPs.
2. The LCD$_{\text{ini}}$ assumes HNPs are rigid spheres, neglecting the possibility that HNPs can significantly change their molecular conformation upon adsorption. The treatment of the spatial distribution of the ligands in the interface is different for LCD$_{\text{ex}}$ and LCD$_{\text{cc}}$. θ_s is the relative maximum occupation of the compact part of EDL, and R is the relative occupation in the first Stern layer (f_{0+1} / ($f_{0+1}+f_2$)). In the LCD$_{\text{ex}}$ model, the fixed value of R leads to $0 < \theta_{\text{S}} < 1$, while in the LCD$_{\text{cc}}$ approach, the ratio R is variable, leading to $0.45 < \theta_{\text{S}} < 1$ (see Section 4.3).
3. In the LCD$_{\text{ini}}$ and LCD$_{\text{ex}}$ models, HNPs are regarded as homogeneous at the particle level having a single affinity with $q = 1$, while the particle-level heterogeneity is introduced in the LCD$_{\text{cc}}$ model with $0 < q < 1$ in Eq. (6), having a median affinity constant ($\widetilde{K}_{\text{o}}$) that follows from calculations with ADAPT module.

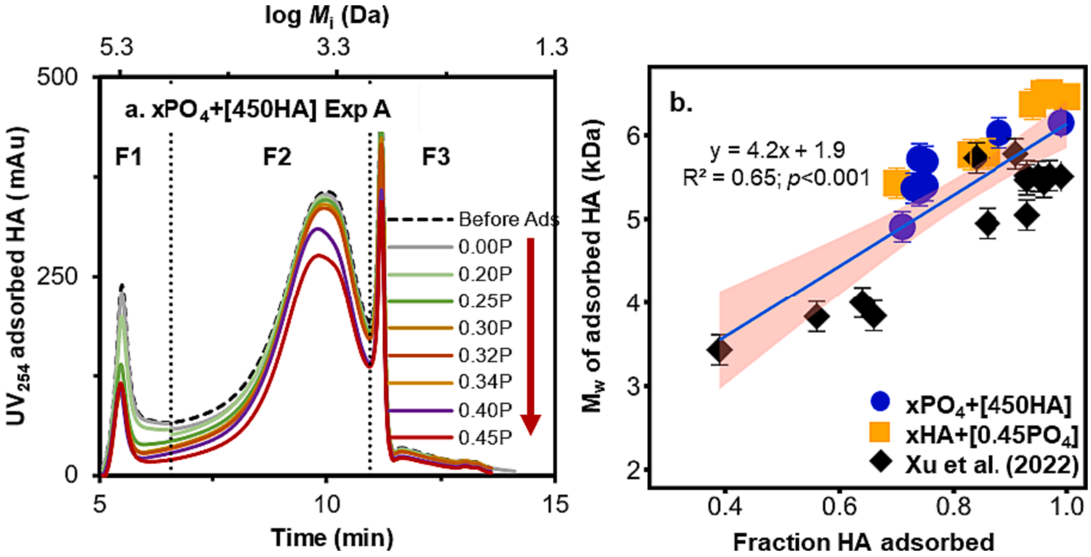

Fig. 2. (a) SEC chromatograms of HA adsorbed by goethite (3 g L^{-1}) in systems with 450 mg HA L^{-1} and various initial phosphate concentrations (0–0.45 mM) in 0.01 M NaCl at pH 4 (noted as xPO_4 + [450HA], Exp A). (b) Mean molar mass (M_w) of adsorbed HA at pH 4 as a function of the fraction adsorbed in Exp A (blue spheres) and Exp B (orange squares). In Fig. 2a, the chromatograms were calculated from the difference in the chromatograms of HA in solution before and after equilibration with goethite. The chromatographs have been divided into three regions, representing three fractions (F1, F2, and F3). The mean molar mass (M_w) in Fig. 2b was calculated with Eq. (1a) using the data of SEC chromatograms from Exp A (Fig. 2a) and Exp B (Fig. S2) of the present study. Diamond symbols were from Xu et al. [17]. The solid line in Fig. 2b is the linear regression for M_w as a function of the fraction of HA adsorbed fitted based on the ordinary least square method [52]. The pink area represents the 95 % confidence interval. The error bar represents the standard deviation of mean M_w of HA (± 0.17 kDa) derived from the chromatograms of HA at different concentrations without adsorption to goethite.

the difference in the chromatograms of HA in solution before and after adsorption. The polydispersity of HA is obvious from the chromatograms, showing a wide range of distribution in particle size. This polydispersity can be expressed by the polydispersity index ρ, which reflects the heterogeneity of the HA particles [37,48]. Fig. 2a shows that the UV light absorbance at 254 nm (UV_{254}) of adsorbed HA decreases with the addition of phosphate, suggesting that less HA is adsorbed due to the competition with phosphate. The polydispersity index (ρ) decreases from 4.6 to 3.5 (Table S1), indicating that the size distribution of adsorbed HA becomes narrower in the presence of phosphate. Certain-sized fractions were preferentially adsorbed in the presence of phosphate. It is expected that the competition with phosphate has led to a stronger preference for HA particles with higher affinity, and these high-affinity particles are more enriched in certain particle size ranges.

For the convenience of the discussion, the chromatograms in Fig. 2a have been divided into three regions around the three peaks, referred to as F1, F2, and F3. The dominant fraction of adsorbed HA is F2, which has a retention time of 6.5 – 11 min (~0.9 – 59 kDa), accounting for 76 ± 2 % of the chromatogram area. With an increase in phosphate loading, the polydispersity index (ρ) of F2 drops from 2.7 to 2.2, and the mean molar mass (M_{w2}) of adsorbed HA in F2 decreases from 7.2 to 5.7 kDa, showing increased preferential adsorption of relatively small-sized HA particles. The sharp peak in the range of 11 – 14 min refers to very small molecules. The mean molar mass of this small fraction of adsorbed HA (F3; on average 15 ± 1 % of the chromatogram area) is about $M_{w3} = 0.6$ kDa (Table S1), reflecting the presence of breakdown products of HA [49–51]. The F1 fraction of adsorbed HA (on average 9 ± 3 % of the chromatogram area) contains rather large molecules with a fairly constant polydispersity ($\rho = 1.15 \pm 0.01$). The mean molar mass is equivalent to ~150 kDa (M_{w1}, Table S1). As suggested by Xu et al. [17], the presence of these moieties may be attributed to the association or aggregation of HA caused by the high ionic strength (0.2 M) of the applied mobile phase. Such aggregation may be weaker or nonexistent in the batch experiments with a background electrolyte level of 0.01 M. Hence, this fraction (F1) has been excluded from the calculation of the mean molar mass (M_w) of adsorbed HA used in Fig. 2b.

As follows from Fig. 2b, the mean molar mass (M_w) systematically decreases as the fraction of HA adsorbed decreases in Exp A, in which the phosphate loading was varied with a fixed HA addition. The same trend is obtained in Exp B in which the HA loading was varied with a fixed phosphate addition. The preferentially adsorbed fraction of the HA contains more aromatic moieties, as revealed by an increase in the $SUVA_{254}$ value of adsorbed HA (Fig. S3). Recently, it has been shown that such aromatic moieties have more functional groups and exhibit a higher affinity for goethite [37]. The preference for certain HA moieties leads to molecular fractionation. The sensitivity of this process can be expressed in a fractionation factor (k), which is the slope of the regression line in Fig. 2b. A similar type of regression between the mean molar mass (M_w) of adsorbed HA and its adsorbed fraction was also found for the batch experiments conducted in the absence of phosphate in our early study [17]. This sensitivity factor (k) is about 4.2 for both data series, i.e., with and without the presence of phosphate. It suggests that the presence of phosphate has a minor effect on the mass fractionation at the same fraction of HA adsorbed. The size selectivity of the HA adsorption mainly depends on the fraction of HA adsorbed. Therefore, the empirical relation, found in single HA adsorption systems [17], can also be applied to model the competition of HA with phosphate, provided that the background electrolyte conditions are the same.

4.2. Analysis of heterogeneity at the particle level

With the LCD framework, the overall affinity K_o can be calculated with the ADAPT module using the mean molar mass (M_w) and the mean density of functional groups (Q_{max}, in mol kg^{-1}) [13]. Concerning the molar mass and size, our previous modeling attempt (LCD_{ex}) did account for the change in the mean molar mass (M_w) of HNPs in the adsorption phase, but ignored a variation around the mean value as measured with SEC (Fig. 2a). In addition, the reactive functional groups are not necessarily homogeneously distributed over the HNPs in terms of types as well as density [19,53–56]. The possible influence of the variation in the density of functional groups will be evaluated in the present modeling.

In the SEC chromatograms, the x-axis is the retention time, which can be interpreted as the logarithm of the molar mass ($\log M_i$) of a certain size fraction. The y-axis of the chromatograms represents the absorbance recorded at 254 nm, which can be used as a measure of the mass concentration (C_p, kg L^{-1}) of HNPs if each size fraction has the same chromophores. It is assumed that each size fraction has its own adsorption affinity ($K_{o,i}$) to oxides under a certain condition.

For HNPs with a discrete size distribution, the overall adsorption, ϕ_{ads}, can be obtained from the summation of the adsorption of different-sized fractions (Eq. (7a)). The frequency (f_i) of each $\log K_{o,i}$ equals the ratio of the corresponding size fraction (i) adsorbed over all the sizes adsorbed (Eq. (7b)).

$$\phi_{ads} = \sum_{i=1}^{n} \phi_{i,ads} \tag{7a}$$

$$f_i = \phi_{i,ads} \Big/ \sum \phi_{i,ads} \tag{7b}$$

Based on the molar mass distribution of adsorbed HNPs measured for Exp A with SEC (Fig. 2a), the HNPs were subdivided into multiple fractions with a certain mean molar mass (M_i). It is assumed that each fraction may have its own specific site density of the functional groups ($Q_{max,j,i}$ with $j = 1$ for carboxylic and $j = 2$ for phenolic groups in the unit of mol kg^{-1}). The corresponding adsorption affinity of each fraction has been calculated with the ADAPT module using M_i and $Q_{max,j,i}$ following Eqs. (5b)–(5d).

If the affinity is continuously distributed, the adsorbed volume fraction ϕ_{ads} of HNPs can be calculated from the integral of the contributions $\phi_{i,ads}$ according to [45,51]:

$$\phi_{ads} = \int_0^{\infty} \phi_{i,ads}\left(\log K_{o,i}, \phi_{sol}\right) f\left(\log K_{o,i}\right) d\left(\log K_{o,i}\right) \tag{8}$$

where $\phi_{i,ads}\left(\log K_{o,i}, \phi_{sol}\right)$ is the local adsorption isotherm (Eq. (5a)), and $f\left(\log K_{o,i}\right)$ is the affinity distribution function, for which a semi-Gaussian distribution can be taken, equating to the equation below [57]:

$$f\left(\log K_{o,i}\right) = \frac{\ln(10)\sin(q\pi)}{\pi\left[\left(\frac{K_i}{\widetilde{K}_o}\right)^{-q} + 2\cos(q\pi) + \left(\frac{K_i}{\widetilde{K}_o}\right)^{q}\right]} \tag{9}$$

where $\widetilde{K}_o$ is the median value of the affinity distribution and the parameter q ($0 < q \leq 1$) determines the width of the distribution of the adsorption affinity of HNPs. For $q = 1$, HNPs behave homogeneous at the particle level, having a single affinity ($\log \widetilde{K}_o$). Introducing Eq. (9) into Eq. (8), the solution of Eq. (8) results in the well-known Langmuir-Freundlich (LF) equation as used in the present model (Eq. (6)).

When optimizing the LCD model, we found that our adsorption data can be best described using the LF approach with a value for the distribution of $q = 0.1$. This value is rather low, indicating that the HNPs vary widely in adsorption affinity. It implies that at the particle level, the heterogeneity is large. This heterogeneity cannot be understood from only a variation in molar mass as measured with SEC. This follows from the calculation of the expected variation in $\log K_o$ as a function of only the molar mass, as measured for the various fractions with SEC. Using this assumption leads to a skewed affinity distribution (Fig. S5a), suggesting that the heterogeneity at the particle level needs an additional explanation. Besides a physical factor, related to particle size/molar mass, HNPs may also vary in the density of the functional groups, in particular the carboxylic groups. This chemical contribution to the particle heterogeneity has been assessed by varying the number of ligands ($N_{max,j=1,l}$) per HNP by adapting the carboxyl group density of each size/molar mass fraction (Eqs. (5c) & (5d)) to achieve a distribution of $\log K_o$ that approaches the distribution according to the adsorption analysis with $q = 0.1$. In this optimization, the density of the phenolic group ($N_{max,j=2,l}$) was kept constant, in agreement with the measurement by Janot et al. [19]. The resulting relationship between the molar mass and the carboxylic group density ($Q_{max,1}$) is given in Fig. 3b with solid-colored symbols. The optimized results show that the carboxylic group densities ($Q_{max,1}$) firstly increase with molar mass (M_w) and then decrease, with the turning points at about $\log M_w \approx 0.5 – 0.7$ ($M_w = 3 – 5$ kDa).

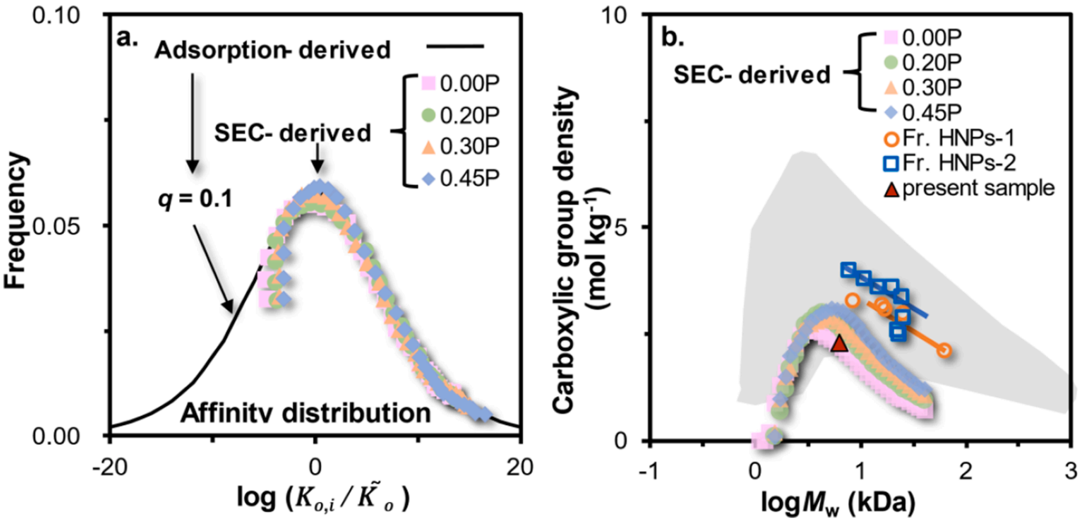

Fig. 3. (a) Relative affinity distribution according to the adsorption data in 0.01 M $NaNO_3$ interpreted with LF model (Eq. (6) using $q = 0.1$ (full line, Eq. (9)) compared to the calculated affinity distribution using the molar mass distribution measured with SEC for adsorption series of Exp A ($x$$PO_4$ + [450HA], pH 4), in combination with an adaptation of the carboxylic group density of each mass fraction (symbols). (b) Relationship between the carboxylic group density ($Q_{max,1}$) and the SEC-measured molar mass ($\log M_w$) of the HNPs in the distribution. The solid-colored symbols represent the $Q_{max,1}$ values of the HNP fractions in our experiment that were derived by fitting the $\log K_o$ values to the affinity distribution according to the LF model with $q = 0.1$ (Fig. 3a). The open orange and blue circles give literature data on measured carboxylic group densities of fractionated HNP, separated respectively by ultrafiltration [54,55] and repeated extraction [58]. The corresponding lines emphasize the negative trend in the relation between $Q_{max,1}$ and $\log M_w$. The red triangle indicates the mean carboxyl group density ($Q_{max,1}$) and mean molar mass ($\log M_w$) of our HNPs. Literature data for non-fractionated HNPs of different origins [30,33,59–61] are also collected (shown as the cloud, details see in Fig. S5b), showing that variation in molar mass ($\log M_w$) and intrinsic carboxylic group density ($Q_{max,1}$) are related, supporting our data analysis.

The relationship between $Q_{\max,1}$ and $\log M_w$ derived from our model evaluation (solid-colored symbols in Fig. 3b) can be compared with literature data (open symbols) [30,33,53–55,58–61]. Christl et al. [54,55] have applied ultrafiltration to fractionate HNPs (orange circles, Fr.HNPs-1) and applied acid-base titrations to reveal the corresponding carboxylic group densities ($Q_{\max,1}$). The range of the M_w of their data is 8.5–63 kDa. As the molar mass of the fractions increased, the values of $Q_{\max,1}$ decreased. Li et al. [58] observed a similar trend for eight HNP fractions (blue circles) with M_w from 7.7 to 25 kDa, obtained by repetitive base extractions of peat soil. The results showed that particles with lower molar masses have higher carboxylic group densities, while the larger ones are primarily composed of aliphatic groups.

In Fig. 3b, we have also evaluated the relation between the carboxylic group density ($Q_{\max,1}$) and the mean molar mass ($\log M_w$) for unfractionated HNPs (shown as the cloud; for details, see Fig. S5b) with literature data [30,33,59–61]. These data cover a wide range of molar mass, ranging from 0.75 to 544 kDa. These results also revealed a negative trend (Fig. 3b) that is in line with our finding, for the fraction with $M_w > \sim 3$ kDa. However, for very small HNPs ($M_w < \sim 3$ kDa), our evaluation suggests the presence of particles with a lower carboxylic group. These particles have a low affinity for adsorption to goethite. A conceivable explanation could be the presence of a small fraction of "neutrals" in the HA with a smaller molar mass, as suggested by Janot et al. [19].

Summarizing the above, our model distinguishes three distinct modes of heterogeneity. The first one is at the level of the functional groups, while the others are at the level of the particles. The chemical heterogeneity resulting from a variation in the intrinsic affinity of the functional groups is treated with the NICA approach by calculating the average chemical state of HNPs in both the solution and adsorption phases. The heterogeneity at the particle level is due to the variation of the molar mass/particle size and a variation in the chemical composition, including the carboxyl density of HNPs. The first one can be considered as the physical mode of particle heterogeneity, while the latter represents the chemical mode of particle heterogeneity. The bell-shaped variation in the density of carboxylic groups, combined with the variation in molar mass measured with SEC, is represented in the LCD model by a single parameter (q) expressing the corresponding variation in the adsorption affinity of HNPs.

4.3. *Evaluating the spatial distribution of reactive functional groups*

In our new modeling approach, the challenge is to simultaneously describe, with a single set of model parameters, the adsorption of HNPs under variable solution and interfacial conditions, such as pH, ionic strength, and the surface loading of HNPs as well as the competitive adsorption of anions such as PO_4^{3-} and others. Exploration shows that, together with the aforementioned heterogeneity at the particle level, the interfacial distribution of the functional groups (or ligands) of HNPs is another crucial factor in the modeling. The molecular conformation of adsorbed HNPs changes with the experimental conditions. In brief, the ligand distribution of flexible molecules is driven by electrostatic forces.

To better investigate the effect of electrostatics on the spatial distribution of the reactive ligands of HA, the modeling results will be evaluated in the absence (Section 4.3.1) and presence (Section 4.3.2) of phosphate as a probe ion. The challenge will be to describe both data sets simultaneously using a single parameter set.

4.3.1. *Humic nanoparticles adsorption without phosphate*

As experienced before [17], the interfacial distribution of reactive ligands of HNPs is pH- and loading-dependent, determining the interfacial gradients of the electrostatic potentials. In our previous modeling approach (LCD_{ex}) [17], the spatial distribution of the HNP ligands in the compact part of the EDL was fixed. A single value was used for the ratio R ($R = 0.5$). However, if all adsorption data (without and with phosphate) from this study are considered simultaneously, the spatial distribution within the Stern layers cannot be fixed to a single value, but is instead found to be condition-dependent.

Our present modeling shows that the molecular conformation of adsorbed HNPs in the compact part of the EDL can be described using a condition-dependent distribution of the reactive ligands over the inner and outer Stern layer (R, Eq. (3b)), in combination with a condition-dependent maximum (θ_s, Eq. (3d)). Both are related to the electrostatic potential profile of the EDL. An initial iterative optimization of the ligand distribution shows that both parameters follow sigmoidal functions of the potential gradients ($\Delta\psi$) in the EDL. The θ_s and R can be approximated arbitrarily by a set of ligand distribution functionals, according to, for instance:

$$\theta_S = \theta_{\min} + \Delta\theta_{\max}\frac{1}{1 + a\,e^{-b\Delta\psi_{02}}} \tag{10a}$$

$$R = R_{\min} + \Delta R_{\max}\frac{1}{1 + c\ e^{-d\Delta\psi_{01}}} \tag{10b}$$

In the above equations, $\theta_{\min}$ and $R_{\min}$ are the minimum values of respectively θ_s and R. These values are relevant at pH close to the PZC of the mineral surface when the electrostatic potential gradients are very small. $\Delta\theta_{\max}$ and $\Delta R_{\max}$ are respectively the maximum increase of θ_s and R that are reached when the electrostatic field is highly attractive. This occurs at low pH. The gradient $\Delta\psi_{02}$ in Eq. (10a) is equal to the electrostatic potential difference between 0- and 2-plane (ψ_0-ψ_2), while $\Delta\psi_{01}$ in Eq. (10b) is equal to the electrostatic potential difference between 0- and 1-plane (ψ_0-ψ_1). The parameters *a, b, c,* and *d* determine the shape of the sigmoidal curves of θ_s and R. By simultaneous fitting of HA adsorption data at a background of 0.01 M $NaNO_3$ (Fig. 4a), those parameters have been optimized.

Fig. 4b shows the maximum adsorption allowed in the Stern layer space (θ_s) as a function of the potential difference over the compact part of the EDL (ψ_0-ψ_2). At a high gradient, the maximum allowed occupation of the Stern layer space approaches the physical maximum, i.e., $\theta_s \sim 1$ implying that $\Delta\theta_s \equiv 1$- $\Delta\theta_{\min}$. Approaching the maximum typically occurs at low pH, where the conditions for binding are favorable. At raising pH, adsorbed HA particles increasingly repel the compact part of the EDL. At high pH, the potential gradient becomes very small, and θ_s then reaches a value close to 0.45. This value points to a surface attachment of the HNPs as spheroidal particles. For spherical particles with a diameter of 2.4 nm and a mean molar mass of ~5.5 kDa (as for the HA adsorbed at 0.01 M), the volume fraction of the spherical cap that overlaps with the Stern layer space is closed to $\theta_s \sim 0.45$, as shown previously [17]. This limit is given in Fig. 4b with a dotted line. Our model suggests that adsorbed HA molecules may exhibit a rather spheroidal shape when the electrostatic forces are small. However, when the electrostatic forces strongly act on the molecules, significant deformation occurs, and the molecules tend to spread out at the surface, allowing for a higher degree of interaction by ligand exchange and charge neutralization by complexation (Fig. 4b).

In Fig. 4c, information is given about the fraction of ligands present in the inner Stern layer relative to the Stern layers (R) as a function of the corresponding electrostatic gradient. At low pH, innersphere complexation is relatively important, stimulated by a large value of ψ_0-ψ_1. At these conditions, the fraction (R) approaches a value of 0.5. At a high pH, there is almost no innersphere complexation with the surface sites, and the ratio R approaches a value of only about 0.1. Under these conditions, with a low gradient of ψ_0-ψ_1, the ligands prefer the outer region of the compact part of the EDL ($f_2 \gg f_{0+1}$).

Constrained by a value for $\theta_{\min}$ based on the spherical cap and using $\Delta\theta_{\max} \equiv 1$- $\theta_{\min}$ and $R_{\min} = 0.1$, the parameters (*a, b, c,* and *d*) for the ligand distribution functionals were optimized using the data collected in a 0.01 M NaCl electrolyte level. Next, both optimized functionals were used to predict the adsorption of HA at a lower (0.002 M) and higher (0.1 M) ionic strengths (Fig. 5). As the mean size of the HA particles depends on the ionic strength [17], the value for $\theta_{\min}$ was adapted

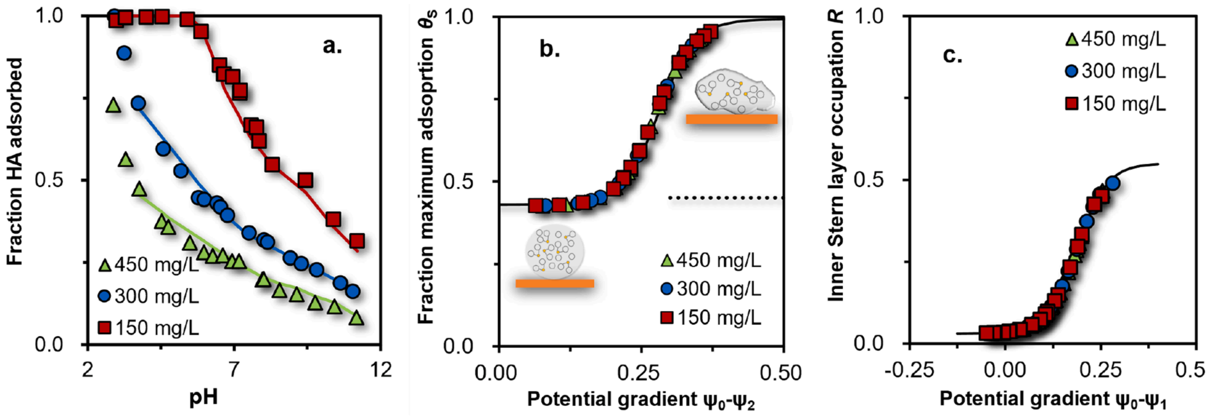

Fig. 4. (a) pH-dependent HA adsorption to goethite measured (Weng et al. [36], symbols) and modeled (lines) with the consistent competitive LCD (LCD_{cc}) model using $q = 0.1$. (b) Relative maximum occupation of the Stern layer (θ_s, Eq. (10a) as a function of potential gradient between 0- and 2-plane (ψ_0-ψ_2). (c) Fraction of reactive ligands in the inner Stern layer over the reactive ligands in the compact part of the EDL (R, Eq. (10b)) as a function of potential gradient between 0- and 1-plane (ψ_0-ψ_1). The results are for goethite (1 g L^{-1}) in 0.01 M $NaNO_3$ at three initial HA loadings, 150 mg/L (squares), 300 mg L^{-1} (circles), and 450 mg L^{-1} (triangles). The dotted line in Fig. 4b refers to the minimum value of θ_s (~0.45). The solid lines in Fig. 4b and 4c have been calculated with the functionals for the ligand distribution of adsorbed HA (Eq. (10)), having minimum and maximum values for θ_s and R, as discussed in the text. Apart from an adjustable conformational change calculated with the functionals of Eq. (10) and a calibrated molecular fractionation (Fig. 2b), the only adjustable parameter in the modeling is the heterogeneity constant ($q = 0.1$) used in the Langmuir-Freundlich approach (Eq. (6)), in which the median affinity constant $\widetilde{K}_o$ has a specific and non-specific contribution calculated with ADAPT module of the LCD_{cc} model. Both affinity constants are calculated using the output of NICA-LD and NICA-Donnan modules.

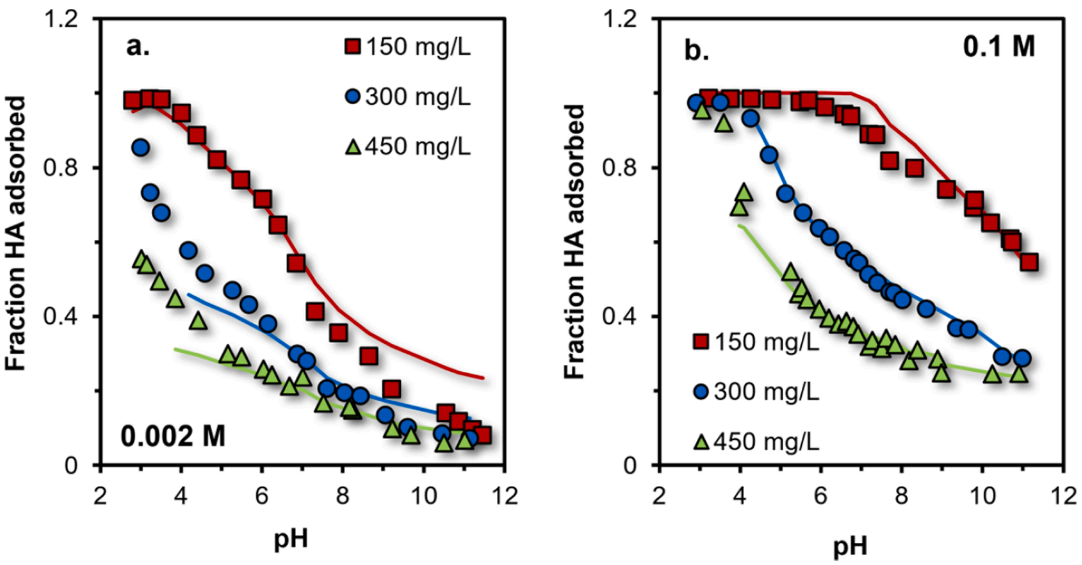

Fig. 5. Adsorption envelopes of HA were measured and calculated with the LCD_{cc} model for three HA loadings (1.0 g L^{-1} goethite) at ionic strength levels of 0.002 M (a) and 0.1 M $NaNO_3$ (b). As the mean molar mass is ionic strength dependent, as derived previously [17], the value of θ_{min} has been correspondingly adapted in the modeling. All other parameters are the same as used for the calculation of the model lines in Fig. 4.

correspondingly to the value calculated for the overlap of a spherical cap with Stern layer space, being $\theta_{min} \sim 0.55$ at 0.002 M $NaNO_3$ and $\theta_{min} \sim 0.35$ at 0.1 M $NaNO_3$. At the highest electrolyte level, the prediction is very good. For the lowest ionic strength, some deviations are present that might be due to differences in molecular conformation and/or fractionation than calculated with the model.

4.3.2. *Competitive adsorption of HA and phosphate*

Fig. 6a depicts the adsorption of HA measured at three HA levels, namely 200 (green), 350 (blue), and 450 (red) mg L^{-1} (symbols) as a function of the phosphate surface loading (Exp A). The corresponding adsorption isotherms of phosphate are given in Fig. 6b.

The solid lines in Fig. 6 are obtained by applying our new LCD framework (LCD_{cc}) with the same parameters as those used in Figs. 4 and 5, having only considered the spatial ligand distribution (θ_s, R) and the width of the affinity distribution of HA particles (q) as the only adjustable parameters (Table 1). These parameters were optimized simultaneously using the datasets for HA adsorption with and without the presence of phosphate.

For a good description of competitive adsorption, it is essential to incorporate particle-level heterogeneity, expressed in the width of the distribution (q) as illustrated in Fig. 7 and Fig. S6. The solid lines in Fig. 7 are for the LCD_{cc} model, while the dashed lines are for the LCD_{ex} model without considering a distribution of affinities of HA particles, i.e., using $q \equiv 1$. In this case, the HA adsorption in the presence of phosphate is strongly underestimated (Fig. 7a). Only by introducing heterogeneity at the particle level can the model simultaneously describe the HA (Fig. 7a) as well as the phosphate adsorption (Fig. 7b) correctly, leading to a realistic description of the spatial distribution of HA ligands with functionals linked to the potential gradients in the EDL.

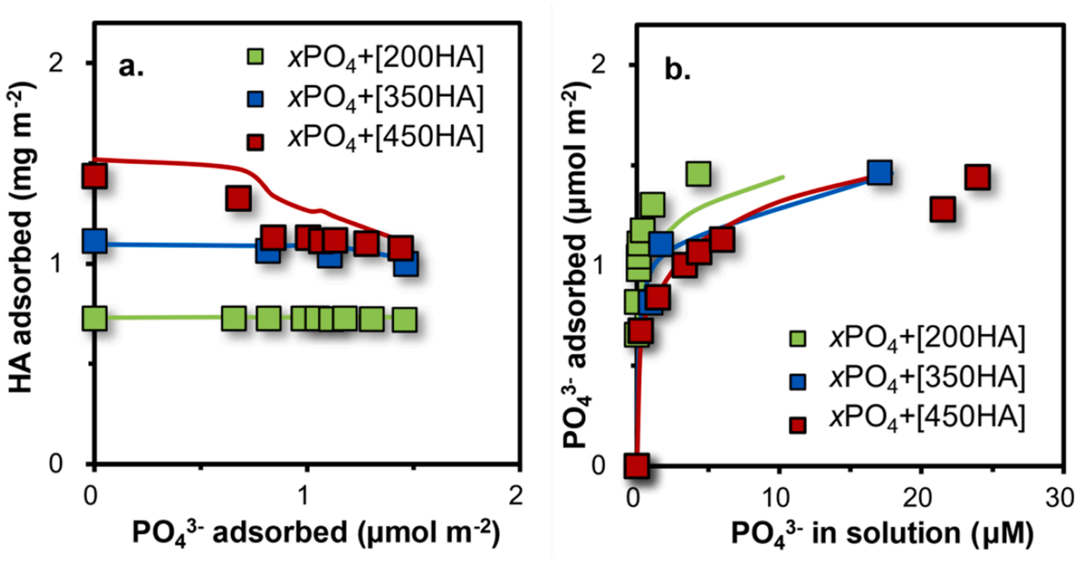

Fig. 6. (a) Adsorbed HA against the phosphate surface loading of goethite (3 g L^{-1}) at pH 4 in 0.01 M NaCl (Exp A). (b) Corresponding adsorption isotherms of phosphate. The phosphate addition (x) varied from 0 to 0.45 mM (indexed as xPO$_4$) at three fixed HA levels of 200 (green), 350 (blue), and 450 (red) mg HA L^{-1}. Symbols: experimental data; Solid lines: LCD$_{cc}$ model applying the same parameter set as used in Figs. 4 and 5. (For interpretation of the references to colour in this figure legend, the reader is referred to the web version of this article.)

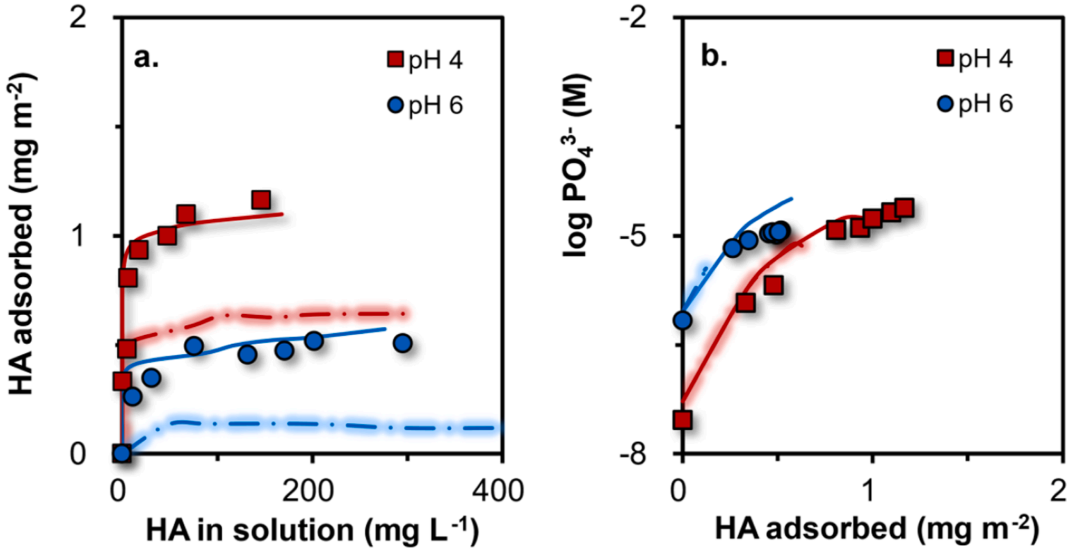

Fig. 7. Effects of particle heterogeneity on modeling HA (a) and phosphate (b) adsorption (given as log PO$_4^{3-}$ in solution) on goethite at pH 4 and 6 (Exp B and C; goethite: 3 g L^{-1}; 0.01 M NaCl). In these experiments, the HA addition varied from 0 to 500 mg L^{-1}, and the phosphate addition was fixed at 0.45 mM. Symbols: experimental data; Solid lines: LCD$_{cc}$ model predictions using the same sets of parameters including $q = 0.1$, as applied in Figs. 4, 5, and 6. Dashed lines: prediction with an extended version of the LCD (LCD$_{ex}$) model without considering particle level heterogeneity ($q \equiv 1$).

5. Conclusions

Humic nanoparticles (HNPs) are a complex mixture of organic molecules that differ in composition and structures [9]. This variation leads to the preferential adsorption of specific fractions of HNPs to (hydr)oxides [18]. The present model (LCD$_{cc}$) has three key factors: (i) variation in the mean molar mass (M_w) of adsorbed HNPs due to fractionation, (ii) spatial distribution of HNPs at the interface, as well as conformational changes of adsorbed HNPs upon changes in solution and surface conditions, and (iii) various modes of HNPs heterogeneity that contribute to the distribution of adsorption affinities.

A novel aspect of the present study is the use of oxyanions to trace the ligand distribution of the HNPs and to create a strong competitive situation that can better reveal the heterogeneity in the adsorption affinity of HNPs. It allows a development of the model for the simultaneous interaction of HNPs and oxyanions with metal (hydr)oxides. As competitive tracers, oxyanions can change the electrostatic gradients in the interface, allowing evaluation of the locations of the charge of adsorbed HNPs. The detected ligand distribution can be expressed in two electrostatic functionals that describe the change in molecular conformation of adsorbed HNPs. In combination with the speciation of the functional groups of HNPS calculated according to the NICA model, the conditional change of the interfacial charge distribution (CD) of the HNPs is derived. Additionally, the model revealed that the heterogeneity of HNPs is not only present at the level of the ligands but also at the level of the particles. These two levels of heterogeneity are treated differently in the LCD$_{cc}$ model. At the level of the ligands, the heterogeneity is described with the NICA approach [16]. At the particle level, heterogeneity is implemented using a semi-Gaussian distribution of affinities around a median value. In the resulting Langmuir-Freundlich adsorption equation only the width of the distribution (q) is an adjustable parameter, while the median affinity ($\widetilde{K}$) is independently calculated by the LCD_{cc} model. The width of the affinity distribution of HNPs at the particle level can be understood from the variation in molar mass and the density of the functional groups.

In the field of colloid and interface chemistry, continuous efforts have been made to understand and model the adsorption of charged soft particles or polyelectrolytes to charged surfaces. The discrete approach [12] treats polyelectrolytes in a similar way to small ions, considering the formation of a limited number of surface species. However, due to the huge variation in the reactive ligands, particle size, and group density of natural HNPs, it is unrealistic to consider all combinations of possible surface species. In other studies, the self-consistent field theory [62] was developed for modeling the adsorption of charged polymers, which considers the spatial distribution of different segments of the adsorbed particles, but the chemical binding of the reactive groups with surface sites is treated as a solvency effect rather than as surface complexation. The LCD model framework for the adsorption of HNPs is an alternative that considers both the continuum distribution of reactive groups and surface complexation [36], using the NICA model to derive a statistical average of surface speciation of the adsorbed particles. Over the last 20 years, the model has been developed in several steps with an increasing number of mechanistic details as summarized in Table 1. However, the earlier models (LCD_{ini} and LCD_{ex}) fail to provide a simultaneous description of the competitive interaction of HNP and oxyanions with metal (hydr)oxides. With the new model developed (LCD_{cc}), the simultaneous adsorption of HNPs and phosphate can be successfully predicted for competitive systems using a minimum and single set of parameters. The insights obtained by the new model can be used to improve the understanding of the adsorption behavior of other types of charged particles present in a variety of technical and natural systems, such as e.g., the adsorption of extracellular polymeric substances (EPS) on minerals [63,64].

CRediT authorship contribution statement

Yun Xu: Writing – review & editing, Writing – original draft, Visualization, Validation, Software, Methodology, Investigation, Formal analysis, Data curation, Conceptualization. **Yilina Bai:** Writing – review & editing, Writing – original draft, Visualization, Validation, Software, Methodology, Investigation, Formal analysis, Data curation, Conceptualization. **Tjisse Hiemstra:** Writing – review & editing, Supervision, Methodology, Conceptualization. **Liping Weng:** Writing – review & editing, Supervision, Software, Resources, Project administration, Methodology, Conceptualization.

Declaration of competing interest

The authors declare that they have no known competing financial interests or personal relationships that could have appeared to influence the work reported in this paper.

Data availability

Data will be made available on request.

Acknowledgments

This work was supported by the China Postdoctoral Science Foundation (2023M741286), the Postdoctoral Fellowship Program of CPSF (GZC20230906), the Science and Technology Innovation Project of Chinese Academy of Agricultural Sciences, the Natural Science Foundation of Tianjin (22JCYBJC00490), the Sandwich Ph.D. scholarship of Wageningen Graduate Schools (WGS), and the Ph.D. scholarship of the China Scholarship Council (CSC). We would also like to give our special acknowledgment to Hans Meeussen for his kind help with ORCHESTRA.

Appendix A. Supplementary data

Supplementary data to this article can be found online at https://doi.org/10.1016/j.jcis.2024.01.078.

References

[1] Y. Bao, N.S. Bolan, J. Lai, Y. Wang, X. Jin, M.B. Kirkham, X. Wu, Z. Fang, Y. Zhang, H. Wang, Interactions between organic matter and Fe (hydr)oxides and their influences on immobilization and remobilization of metal(loid)s: A Review, Crit. Rev. Environ. Sci. Technol. 52 (2022) 4016–4037, https://doi.org/10.1080/10643389.2021.1974766.

[2] Y. Cui, X. Du, L. Weng, W.H. Van Riemsdijk, Assessment of in situ immobilization of lead (Pb) and arsenic (As) in contaminated soils with phosphate and iron: Solubility and bioaccessibility, Water Air Soil Pollut. 213 (2010) 95–104, https://doi.org/10.1007/s11270-010-0370-8.

[3] E. Hoffland, T.W. Kuyper, R.N.J. Comans, R.E. Creamer, Eco-functionality of organic matter in soils, Plant Soil. 455 (2020) 1–22, https://doi.org/10.1007/s11104-020-04651-9.

[4] A. Aftabtalab, J. Rinklebe, S.M. Shaheen, N.K. Niazi, E. Moreno-Jiménez, J. Schaller, K.-H. Knorr, Review on the interactions of arsenic, iron (oxy)(hydr)oxides, and dissolved organic matter in soils, sediments, and groundwater in a ternary system, Chemosphere 286 (2022) 131790, https://doi.org/10.1016/j.chemosphere.2021.131790.

[5] E.M. Peña-Méndez, J. Havel, J. Patočka, Humic substances - compounds of still unknown structure: Applications in agriculture, industry, environment, and biomedicine, J. Appl. Biomed. 3 (2005) 13–24, https://doi.org/10.32725/jab.2005.002.

[6] L. Li, M. Fan, R.C. Brown, J. (Hans) Van Leeuwen, J. Wang, W. Wang, Y. Song, P. Zhang, Synthesis, properties, and environmental applications of nanoscale iron-based materials: A review, Crit. Rev. Environ. Sci. Technol. 36 (2006) 405–431, https://doi.org/10.1080/10643380600620387.

[7] M. Safiur Rahman, M. Whalen, G.A. Gagnon, Adsorption of dissolved organic matter (DOM) onto the synthetic iron pipe corrosion scales (goethite and magnetite): effect of pH, Chem. Eng. J. 234 (2013) 149–157, https://doi.org/10.1016/j.cej.2013.08.077.

[8] J.P. Pinheiro, E. Rotureau, J.F.L. Duval, Addressing the electrostatic component of protons binding to aquatic nanoparticles beyond the Non-Ideal Competitive Adsorption (NICA)-Donnan level: theory and application to analysis of proton titration data for humic matter, J. Colloid Interface Sci. 583 (2021) 642–651, https://doi.org/10.1016/j.jcis.2020.09.059.

[9] E.K. Coward, T. Ohno, D.L. Sparks, Direct evidence for temporal molecular fractionation of dissolved organic matter at the iron oxyhydroxide interface, Environ. Sci. Tech. 53 (2019) 642–650, https://doi.org/10.1021/acs.est.8b04687.

[10] M.J. Avena, L.K. Koopal, W.H. Van Riemsdijk, Proton binding to humic acids: electrostatic and intrinsic interactions, J. Colloid Interface Sci. 217 (1999) 37–48, https://doi.org/10.1006/jcis.1999.6317.

[11] P. Lodeiro, C. Rey-Castro, C. David, E.P. Achterberg, J. Puy, M. Gledhill, Acid-base properties of dissolved organic matter extracted from the marine environment, Sci. Total Environ. 729 (2020) 138437, https://doi.org/10.1016/j.scitotenv.2020.138437.

[12] J.D. Filius, D.G. Lumsdon, J.C.L. Meeussen, T. Hiemstra, W.H. Van Riemsdijk, Adsorption of fulvic acid on goethite, Geochim. Cosmochim. Acta 64 (2000) 51–60, https://doi.org/10.1016/S0016-7037(99)00176-3.

[13] L. Weng, W.H. Van Riemsdijk, L.K. Koopal, T. Hiemstra, Ligand and Charge Distribution (LCD) model for the description of fulvic acid adsorption to goethite, J. Colloid Interface Sci. 302 (2006) 442–457, https://doi.org/10.1016/j.jcis.2006.07.005.

[14] T. Saito, L.K. Koopal, S. Nagasaki, S. Tanaka, Adsorption of heterogeneously charged nanoparticles on a variably charged surface by the extended surface complexation approach: charge regulation, chemical heterogeneity, and surface complexation, J. Phys. Chem. B. 112 (2008) 1339–1349, https://doi.org/10.1021/jp076621x.

[15] Y. Liang, Y. Ding, P. Wang, G. Lu, Z. Dang, Z. Shi, Modeling sorptive fractionation of organic matter at the mineral-water interface, Soil Sci. Soc. Am. J. 83 (2019) 107–117, https://doi.org/10.2136/sssaj2018.07.0275.

[16] D.G. Kinniburgh, C.J. Milne, M.F. Benedetti, J.P. Pinheiro, J. Filius, L.K. Koopal, W. H. Van Riemsdijk, Metal ion binding by humic acid: application of the NICA-Donnan model, Environ. Sci. Tech. 30 (1996) 1687–1698, https://doi.org/10.1021/es950695h.

[17] Y. Xu, T. Hiemstra, W. Tan, Y. Bai, L. Weng, Key factors in the adsorption of natural organic matter to metal (hydr)oxides: fractionation and conformational change, Chemosphere 308 (2022) 136129, https://doi.org/10.1016/j.chemosphere.2022.136129.

[18] J. Hur, M.A. Schlautman, Molecular weight fractionation of humic substances by adsorption onto minerals, J. Colloid Interface Sci. 264 (2003) 313–321, https://doi.org/10.1016/S0021-9797(03)00444-2.

[19] N. Janot, P.E. Reiller, X. Zheng, J.-P. Croué, M.F. Benedetti, Characterization of humic acid reactivity modifications due to adsorption onto α-Al2O3, Water Res. 46 (2012) 731–740, https://doi.org/10.1016/j.watres.2011.11.042.

[20] X. Qin, F. Liu, G. Wang, H. Hou, F. Li, L. Weng, Fractionation of humic acid upon adsorption to goethite: Batch and column studies, Chem. Eng. J. 269 (2015) 272–278, https://doi.org/10.1016/j.cej.2015.01.124.

[21] H. Xu, L. Ji, M. Kong, H. Jiang, J. Chen, Molecular weight-dependent adsorption fractionation of natural organic matter on ferrihydrite colloids in aquatic environment, Chem. Eng. J. 363 (2019) 356–364, https://doi.org/10.1016/j.cej.2019.01.154.

[22] I. Ko, J.-Y. Kim, K.-W. Kim, Adsorption properties of soil humic and fulvic acids by hematite, Chem. Spec. Bioavailab. 17 (2005) 41–48, https://doi.org/10.3184/095422905782774928.

[23] S. Avneri-Katz, R.B. Young, A.M. McKenna, H. Chen, Y.E. Corilo, T. Polubesova, T. Borch, B. Chefetz, Adsorptive fractionation of dissolved organic matter (DOM) by mineral soil: macroscale approach and molecular insight, Org Geochem. 103 (2017) 113–124, https://doi.org/10.1016/j.orggeochem.2016.11.004.

[24] P. Reiller, B. Amekraz, C. Moulin, Sorption of Aldrich humic acid onto hematite: Insights into fractionation phenomena by electrospray ionization with Quadrupole Time-of-Flight Mass Spectrometry, Environ. Sci. Tech. 40 (2006) 2235–2241, https://doi.org/10.1021/es0520518.

[25] F. Claret, T. Schäfer, J. Brevet, P.E. Reiller, Fractionation of Suwannee River fulvic acid and Aldrich humic acid on α-Al2O3: spectroscopic evidence, Environ. Sci. Tech. 42 (2008) 8809–8815, https://doi.org/10.1021/es801257g.

[26] C.V. Waiman, J.M. Arroyave, H. Chen, W. Tan, M.J. Avena, G.P. Zanini, The simultaneous presence of glyphosate and phosphate at the goethite surface as seen by XPS, ATR-FTIR and competitive adsorption isotherms, Colloids Surf. A Physicochem. Eng. Asp. 498 (2016) 121–127, https://doi.org/10.1016/j.colsurfa.2016.03.049.

[27] T. Hiemstra, W. Zhao, Reactivity of ferrihydrite and ferritin in relation to surface structure, size, and nanoparticle formation studied for phosphate and arsenate, environmental science, Nano 3 (2016) 1265–1279, https://doi.org/10.1039/C6EN00061D.

[28] Z. Ajmal, A. Muhmood, M. Usman, S. Kizito, J. Lu, R. Dong, S. Wu, Phosphate removal from aqueous solution using iron oxides: adsorption, desorption and regeneration characteristics, J. Colloid Interface Sci. 528 (2018) 145–155, https://doi.org/10.1016/j.jcis.2018.05.084.

[29] J. Hur, M.A. Schlautman, Effects of pH and phosphate on the adsorptive fractionation of purified Aldrich humic acid on kaolinite and hematite, J. Colloid Interface Sci. 277 (2004) 264–270, https://doi.org/10.1016/j.jcis.2004.04.046.

[30] T. Hiemstra, S. Mia, P.-B. Duhaut, B. Molleman, Natural and pyrogenic humic acids at goethite and natural oxide surfaces interacting with phosphate, Environ. Sci. Tech. 47 (2013) 9182–9189, https://doi.org/10.1021/es400997n.

[31] A.W. Chassé, T. Ohno, Higher molecular mass organic matter molecules compete with orthophosphate for adsorption to iron (oxy)hydroxide, Environ. Sci. Tech. 50 (2016) 7461–7469, https://doi.org/10.1021/acs.est.6b01582.

[32] J.M. Arroyave, C.C. Waiman, G.P. Zanini, M.J. Avena, Effect of humic acid on the adsorption/desorption behavior of glyphosate on goethite. Isotherms and kinetics, Chemosphere 145 (2016) 34–41, https://doi.org/10.1016/j.chemosphere.2015.11.082.

[33] Y. Deng, L. Weng, Y. Li, J. Ma, Y. Chen, Understanding major NOM properties controlling its interactions with phosphorus and arsenic at goethite-water interface, Water Res. 157 (2019) 372–380, https://doi.org/10.1016/j.watres.2019.03.077.

[34] J. Schellekens, P. Buurman, K. Kalbitz, A.V. Zomeren, P. Vidal-Torrado, C. Cerli, R. N.J. Comans, Molecular features of humic acids and fulvic acids from contrasting environments, Environ. Sci. Tech. 51 (2017) 1330–1339, https://doi.org/10.1021/acs.est.6b03925.

[35] T. Hiemstra, W.H. Van Riemsdijk, G.H. Bolt, Multisite proton adsorption modeling at the solid/solution interface of (hydr)oxides: a new approach, J. Colloid Interface Sci. 133 (1989) 91–104, https://doi.org/10.1016/0021-9797(89)90284-1.

[36] L. Weng, W.H. Van Riemsdijk, T. Hiemstra, Adsorption of humic acids onto goethite: effects of molar mass, pH and ionic strength, J. Colloid Interface Sci. 314 (2007) 107–118, https://doi.org/10.1016/j.jcis.2007.05.039.

[37] L. Wang, Y. Li, L. Weng, Y. Sun, J. Ma, Y. Chen, Using chromatographic and spectroscopic parameters to characterize preference and kinetics in the adsorption of humic and fulvic acid to goethite, Sci. Total Environ. 666 (2019) 766–777, https://doi.org/10.1016/j.scitotenv.2019.02.235.

[38] J.C.L. Meeussen, ORCHESTRA: an object-oriented framework for implementing chemical equilibrium models, Environ. Sci. Tech. 37 (2003) 1175–1182, https://doi.org/10.1021/es025597s.

[39] W. Tan, J. Xiong, Y. Li, M. Wang, L. Weng, L.K. Koopal, Proton binding to soil humic and fulvic acids: experiments and NICA-Donnan modeling, Colloids Surf. A: Physicochem. Eng. Asp. 436 (2013) 1152–1158, https://doi.org/10.1016/j.colsurfa.2013.08.010.

[40] L. Weng, W.H. Van Riemsdijk, T. Hiemstra, Humic nanoparticles at the oxide−water interface: interactions with phosphate ion adsorption, Environ. Sci. Tech. 42 (2008) 8747–8752, https://doi.org/10.1021/es801631d.

[41] D.L. Chapman, A contribution to the theory of electrocapillarity, Phil. Mag. 25 (1913) 475–481, https://doi.org/10.1080/14786440408634187.

[42] G. Sposito, Gouy-Chapman Theory, in: W.M. White (Ed.), Encyclopedia of Geochemistry, Springer International Publishing, Cham, 2016, pp. 1–6, https://doi.org/10.1007/978-3-319-39193-9_50-1.

[43] T. Hiemstra, W.H. Van Riemsdijk, A surface structural approach to ion adsorption: the Charge Distribution (CD) model, J. Colloid Interface Sci. 179 (1996) 488–508, https://doi.org/10.1006/jcis.1996.0242.

[44] J. Xiong, L. Weng, L.K. Koopal, M. Wang, Z. Shi, L. Zheng, W. Tan, Effect of soil fulvic and humic acids on Pb binding to the goethite/solution interface: ligand Charge Distribution modeling and speciation distribution of Pb, Environ. Sci. Tech. 52 (2018) 1348–1356, https://doi.org/10.1021/acs.est.7b05412.

[45] J.C.M. De Wit, W.H. Van Riemsdijk, L.K. Koopal, Proton binding to humic substances. 1. Electrostatic effects, Environ. Sci. Tech. 27 (1993) 2005–2014, https://doi.org/10.1021/es00047a004.

[46] J.W. Birkett, M.N. Jones, N.D. Bryan, F.R. Livens, Computer modelling of partial specific volumes of humic substances, Eur. J. Soil Sci. 48 (1997) 131–137, https://doi.org/10.1111/j.1365-2389.1997.tb00192.x.

[47] L. Koopal, W. Tan, M. Avena, Equilibrium mono- and multicomponent adsorption models: from homogeneous ideal to heterogeneous non-ideal binding, Adv. Colloid Interface Sci. 280 (2020) 102138, https://doi.org/10.1016/j.cis.2020.102138.

[48] S. Kang, B. Xing, Humic acid fractionation upon sequential adsorption onto goethite, Langmuir 24 (2008) 2525–2531, https://doi.org/10.1021/la702914q.

[49] S. Rosenberger, C. Laabs, B. Lesjean, R. Gnirss, G. Amy, M. Jekel, J.-C. Schrotter, Impact of colloidal and soluble organic material on membrane performance in membrane bioreactors for municipal wastewater treatment, Water Res. 40 (2006) 710–720, https://doi.org/10.1016/j.watres.2005.11.028.

[50] S. Liu, M. Lim, R. Fabris, C.W.K. Chow, M. Drikas, G. Korshin, R. Amal, Multi-wavelength spectroscopic and chromatography study on the photocatalytic oxidation of natural organic matter, Water Res. 44 (2010) 2525–2532, https://doi.org/10.1016/j.watres.2010.01.036.

[51] M. Yu, X. He, J. Liu, Y. Wang, B. Xi, D. Li, H. Zhang, C. Yang, Characterization of isolated fractions of dissolved organic matter derived from municipal solid waste compost, Sci. Total Environ. 635 (2018) 275–283, https://doi.org/10.1016/j.scitotenv.2018.04.140.

[52] S.V.C. De Souza, R.G. Junqueira, A procedure to assess linearity by ordinary least squares method, Anal. Chim. Acta 552 (2005) 25–35, https://doi.org/10.1016/j.aca.2005.07.043.

[53] H. Shin, Spectroscopic and chemical characterizations of molecular size fractionated humic acid, Talanta 50 (1999) 641–647, https://doi.org/10.1016/S0039-9140(99)00161-7.

[54] I. Christl, H. Knicker, I. Kögel-Knabner, R. Kretzschmar, Chemical heterogeneity of humic substances: characterization of size fractions obtained by hollow-fibre ultrafiltration, Eur. J. Soil Sci. 51 (2000) 617–625, https://doi.org/10.1111/j.1365-2389.2000.00352.x.

[55] I. Christl, R. Kretzschmar, Interaction of copper and fulvic acid at the hematite-water interface, Geochim. Cosmochim. Acta 65 (2001) 3435–3442, https://doi.org/10.1016/S0016-7037(01)00695-0.

[56] M. Khalaf, S.D. Kohl, E. Klumpp, J.A. Rice, E. Tombácz, Comparison of sorption domains in molecular weight fractions of a soil humic acid using Solid-State ^{19}F NMR, Environ. Sci. Tech. 37 (2003) 2855–2860, https://doi.org/10.1021/es0206386.

[57] J.C.M. De Wit, W.H. Van Riemsdijk, M.M. Nederlof, D.G. Kinniburgh, L.K. Koopal, Analysis of ion binding on humic substances and the determination of intrinsic affinity distributions, Anal. Chim. Acta 232 (1990) 189–207, https://doi.org/10.1016/S0003-2670(00)81235-0.

[58] L. Li, W. Huang, P. Peng, G. Sheng, J. Fu, Chemical and molecular heterogeneity of humic acids repetitively extracted from a peat, Soil Sci. Soc. Am. J. 67 (2003) 740–746, https://doi.org/10.2136/sssaj2003.7400.

[59] J.D. Ritchie, E.M. Perdue, Analytical constraints on acidic functional groups in humic substances, Org. Geochem. 39 (2008) 783–799, https://doi.org/10.1016/j.orggeochem.2008.03.003.

[60] M.M.D. Sierra, M. Giovanela, E. Parlanti, V.I. Esteves, A.C. Duarte, A. Fransozo, E. J. Soriano-Sierra, Structural description of humic substances from subtropical coastal environments using elemental analysis, FT-IR and ^{13}C-Solid State NMR data, J. Coast. Res. 42 (2005) 370–382. http://www.jstor.org/stable/25737004.

[61] T. Shinozuka, M. Shibata, T. Yamaguchi, Molecular weight characterization of humic substances by MALDI-TOF-MS, J. Mass Spectrometry Soc. Jpn. 52 (2004) 29–32, https://doi.org/10.5702/massspec.52.29.

[62] A.W.P. Vermeer, F.A.M. Leermakers, L.K. Koopal, Adsorption of weak polyelectrolytes on surfaces with a variable charge. Self-Consistent-Field Calculations, Langmuir 13 (1997) 4413–4421, https://doi.org/10.1021/la9701440.

[63] A. Omoike, J. Chorover, Adsorption to goethite of extracellular polymeric substances from Bacillus subtilis, Geochim. Cosmochim. Acta 70 (2006) 827–838, https://doi.org/10.1016/j.gca.2005.10.012.

[64] L. Fang, Q. Huang, X. Wei, W. Liang, X. Rong, W. Chen, P. Cai, Microcalorimetric and potentiometric titration studies on the adsorption of copper by extracellular polymeric substances (EPS), minerals and their composites, Bioresour. Technol. 101 (2010) 5774–5779, https://doi.org/10.1016/j.biortech.2010.02.075.